Citation: Rane, S., Kovačević, A. & Read, M. (2024). Development of Numerical Grid and CFD Model for Analysis of Oil-Injected IGSM. Paper presented at the 13th International Conference on Compressors and Their Systems, 11-13 Sep 2023, London, UK. doi: 10.1007/978-3-031-42663-6_41

Development of Numerical Grid and CFD Model for Analysis of Oil-injected IGSM

Sham Rane, Ahmed Kovačević and Matthew Read

City, University of London, London EC1V 0HB, UK
sham.rane@city.ac.uk

Abstract. A novel prototype design of an internally geared twin screw compressor for air, with oil injection has been analysed using a custom developed numerical grid. A two-fluid Eulerian-Eulerian CFD model has been applied for the calculations. Compressor performance at various operating conditions has been evaluated together with an analysis of the flow at the suction, discharge, and injection ports. Over the calculated range of speed and pressure, a specific power of 2 – 4 kW/m^3/min was estimated with a maximum volumetric efficiency of 95%. The adopted CFD model could be further used to optimize the oil injection and evaluate design modifications such as rotor profiles, variable lead rotors, etc.

Keywords: CFD, Dynamic Mesh, Screw Compressor, Oil Injection, IGSM.

1 Introduction

A novel design of a positive displacement compressor is the internally geared configuration. In this arrangement, the conventional compressor housing is eliminated, and the second screw rotor is internally lobed in a conjugate action with the inner conventional screw rotor. To improve the volumetric and adiabatic efficiency of the compressor, oil is injected during the compression process. Numerical models using CFD can be used to evaluate such oil injection design and help in achieving an improved performance at various operating conditions.

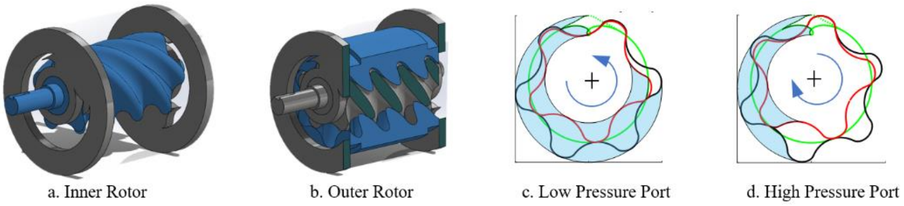
a. Inner Rotor
b. Outer Rotor
c. Low Pressure Port
d. High Pressure Port

Fig. 1. Prototype model of 5-6 IGSC with end plates showing the suction and discharge ports.

Fig. 1 shows the layout of a 5-6 configuration that is being prototyped [1, 2]. Two end plates house the bearings for the 5-lobed inner rotor and have cut-outs for the suction and discharge port. The 6-lobed outer rotor is also rotating about an offset parallel axis, and it is held within a housing not shown here. The port shapes are important for controlling the closing of suction and opening of discharge, also to avoid any direct connection between the two ends.

A design procedure for IGSM for applications to compressors has been reported in [1]. The parameters such as flow rate, flow velocity in the ports were considered. A more detailed evaluation of such rotor geometry is presented in [2]. Swept volume, port flow areas and leakage areas were studied with respect to the rotor's geometrical variation such as profile and wrap angles. Respective advantages of IGSM were identified.

In this work, an in-house grid generator tool SCORG has been used for generating the computational grid of the deforming rotor domain. A two-fluid Eulerian-Eulerian model has been applied for calculations of oil injection during the compression process. Compressor performance such as flow, indicated power, efficiencies at various operating conditions have been evaluated. Additionally, the suction and discharge port configuration has been studied for timing, filling, and built-in compression characteristics.

2 Grid Generation for Internally Geared Screw Rotors

2.1 Rotor Grid Generation Procedure

The rotor grid generation has been implemented in the customised grid generator SCORG [3]. The procedure uses a combination of analytical and differential mesh generation. The cross-section grid is controlled using a distribution factor, number of nodes on the profile and in the radial space. Fig. 2 represents the main steps in the generation of the 2D cross section mesh. By setting an angular increment to the rotor movement, the time advancement of the grid nodes and helical shape of the rotor is obtained [3].

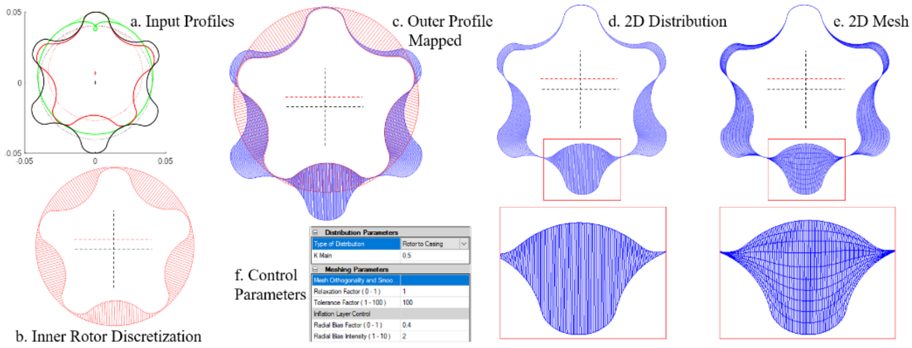

Distribution Parameters	
Type of Distribution	Rotor to Casing
K Main	0.5
Meshing Parameters	
Mesh Orthogonality and Smoo...	
Relaxation Factor (0 - 1)	1
Tolerance Factor (1 - 100)	100
Inflation Layer Control	
Radial Bias Factor (0 - 1)	0.4
Radial Bias Intensity (1 - 10)	2

Fig. 2. Procedure of the rotor grid generation in the cross-section and control parameters.

2.2 Profile Adaptability

The developed grid generator can adapt to profile variations such as shapes, different lobe combinations, depth of chambers, axis offset and wrap angles. Fig. 3 shows three examples of 2-3, 4-5 and 8-9 lobes with small differences in profile parameters. The corresponding IGSM applications can range from low pressure ratio blowers to Gerotor type liquid pumps [1].

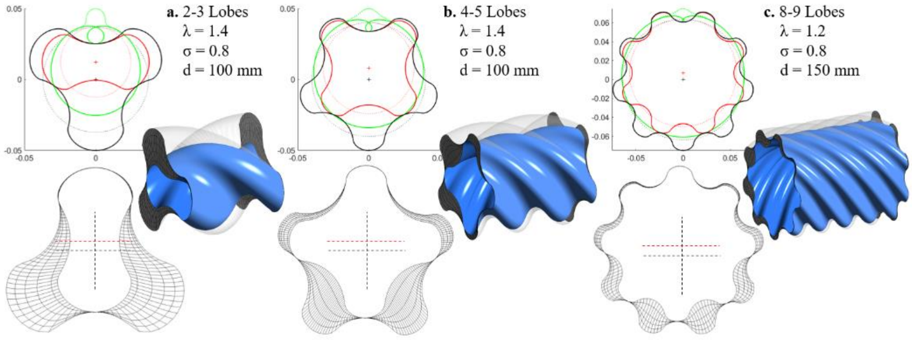

Fig. 3. Few examples of IGSM rotor profiles and cross-section grid.

2.3 Lead Variation

Another type of rotor design variation under investigation is its lead. By applying a variable lead on the IGSM rotors, it will be feasible to eliminate the ports, while still achieving the built-in compression ratio. A relative advantage is offered for bearing sizing and arrangement, etc. The CFD model was required to be capable of evaluation of such design variations, for which the rotor grid generator has been adopted. Using rotor lead variation, the axial spacing between the cross-section grids is calculated and the 3D grid is modified [4]. The 2D grid data remains the same as it was for an unform lead rotor. Fig. 4 shows two examples of lead variations. In Fig. 4a, the low-pressure end pitch is 80 mm and that at the high-pressure end is 20 mm, there-by reducing the lobe spacing axially. In Fig. 4b, this has been reduced further to 10mm. In both cases, the wrap angle of the rotor increases proportionally.

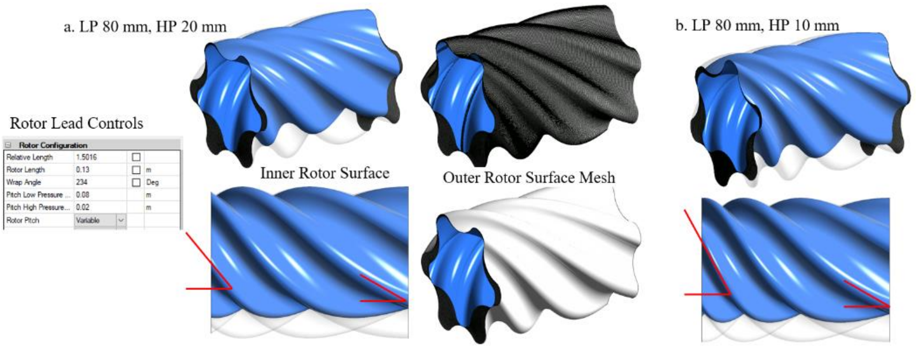

Rotor Configuration

Relative Length	1.5016	☐	
Rotor Length	0.13	☐	m
Wrap Angle	234	☐	Deg
Pitch Low Pressure ...	0.08		m
Pitch High Pressure...	0.02		m
Rotor Pitch	Variable		

Fig. 4. Examples of lead variation on the IGSM rotors.

3 CFD Model of Oil Injected IGSC

Unlike the classical twin screw compressor, where the housing is available for positioning the oil injection ports, in case of IGSM's the outer rotor poses a challenge to design the oil injection system. In this case study, the prototype IGSM was evaluated with an oil injection located on the high-pressure end plate. The injection was timed to begin at 30 degrees past the suction closure. Table 1 presents the main parameters of the prototype design and Fig. 5 represents the CFD model. Main parts of the CFD model are the rotors, suction, discharge, and oil injection ports. Additionally axial gaps were introduced. The operating clearance between the rotors was specified as 100 µm, the axial clearance at suction side was set at 100 µm and that at the discharge end was set at 50 µm. Oil injection hole size was 5 mm and the injection pressure was set to be equal to the discharge pressure.

Table 1. The 5-6 IGSC prototype design.

Variable	Value	Description
N_1 (-)	6	Outer rotor lobe number
N_2 (-)	5	Inner rotor lobe number
D (mm)	100	Diameter of outer rotor
L (mm)	130	Length of both rotors
E (mm)	6.712	Axis spacing distance
λ (-)	1.4	Profile shape parameters
$\bar{\sigma}$ (-)	0.8	
$\bar{\Phi}$ (deg)	234	Wrap angle
ϵ_v (-)	2	Built-in volume ratio

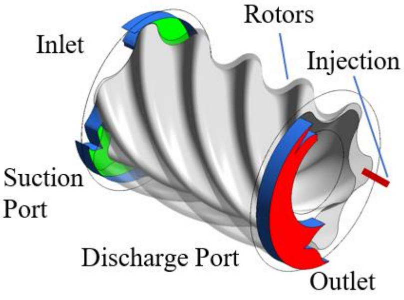

Fig. 5. Schematic of the CFD Model

The description of the two fluid CFD model suitable for oil injected compressors has been reported in [5]. The same parameters for the solver, air and oil properties have been used. Table 2 shows the main settings of the ANSYS CFX solver.

Table 2. ANSYS CFX Solver setup.

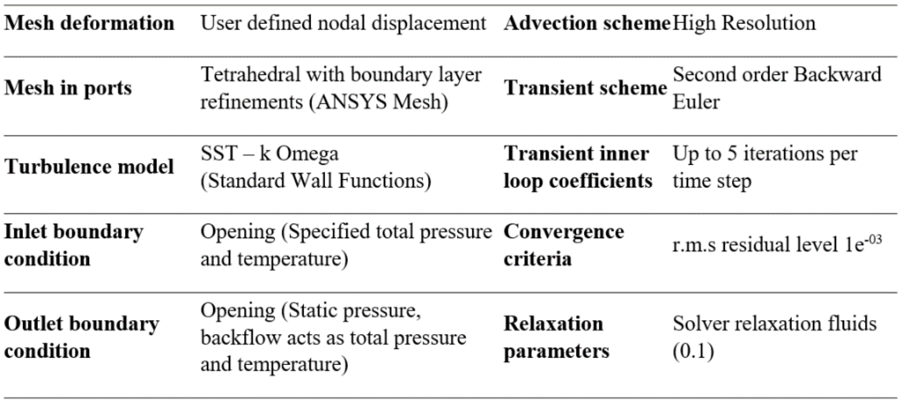

Mesh deformation	User defined nodal displacement	**Advection scheme**	High Resolution
Mesh in ports	Tetrahedral with boundary layer refinements (ANSYS Mesh)	**Transient scheme**	Second order Backward Euler
Turbulence model	SST – k Omega (Standard Wall Functions)	**Transient inner loop coefficients**	Up to 5 iterations per time step
Inlet boundary condition	Opening (Specified total pressure and temperature)	**Convergence criteria**	r.m.s residual level 1e^{-03}
Outlet boundary condition	Opening (Static pressure, backflow acts as total pressure and temperature)	**Relaxation parameters**	Solver relaxation fluids (0.1)

4 Results and Discussion

The test compressor was analysed over a speed range of 1000 to 4000 rpm and at two discharge pressures of 200 and 300 kPa. At the suction, the pressure was set at 100 kPa and temperature of 25 °C. The oil injection pressure was set equal to the discharge pressure and temperature of 40 °C. The results have been presented here to study the characteristics of compression and interaction of injected oil during the cycles.

4.1 Pressure Distribution

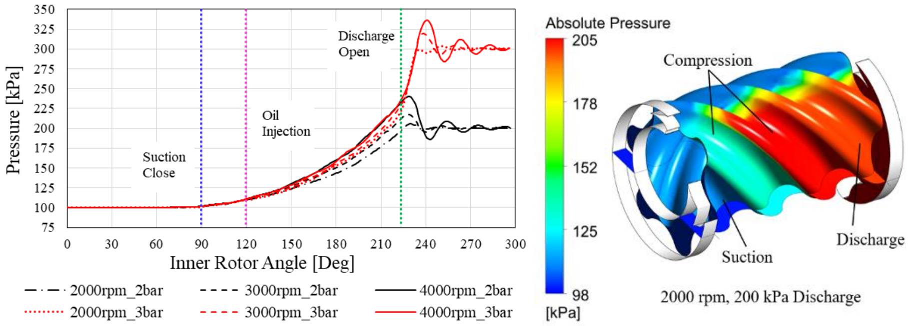

Fig. 6. Chamber pressure variation with rotor angle and a sample instantaneous distribution.

The variation of pressure in the chamber with rotation of the inner rotor is presented in Fig. 6 at different operating conditions. An instantaneous distribution of pressure on the inner rotor has also been shown at 2000 rpm and 200 kPa discharge pressure. The suction port is closed at 90°. Oil injection starts at 120° inner rotor angle and for a built-in volume index of 2.0, the discharge port opens at 220° inner rotor angle. It can be observed that for 200 kPa and 2000 rpm, the internal pressure rise matches the discharge pressure. With increase of speed, over-compression is seen. At higher pressure of 300 kPa, there is under-compression when the port opens. The pressure continues to rise with further rotor rotation and the peak is about 25 kPa higher at 4000 rpm.

4.2 Rotor Torque Variation

The 5-6 profile of the test compressor was designed such that transmission torque is minimum. Under ideal conditions the outer rotor is running free with zero torque. However, due to leakage and diffusion of pressure across adjacent chambers, there is a resultant transmission torque. This has been evaluated from the CFD model. Fig. 7 presents the cyclic variation of torque on the inner and outer rotor with rotation angle of the inner rotor. Due to five lobes on the inner rotor, a full rotation consists of five cycles.

For the inner rotor, which is the main drive element, the torque at 200 kPa, 2000 rpm is 2.5 Nm. With higher speed of 4000 rpm, there is an increase in the torque to 3.0 Nm. This is related to the over-compression seen in the pressure distribution plot of Fig. 6.

At 300 kPa discharge pressure the average torque increases to 4.5 Nm. The difference between the two speeds reduces. In case of the outer rotor, relatively there is a lower average torque. At 200 kPa, 2000 rpm, it is 1.75 Nm, and a small increase is seen at 4000 rpm. At 300 kPa, 2000 rpm, the average torque increases to 2.0 Nm and at 4000 rpm it further increases to 2.25 Nm.

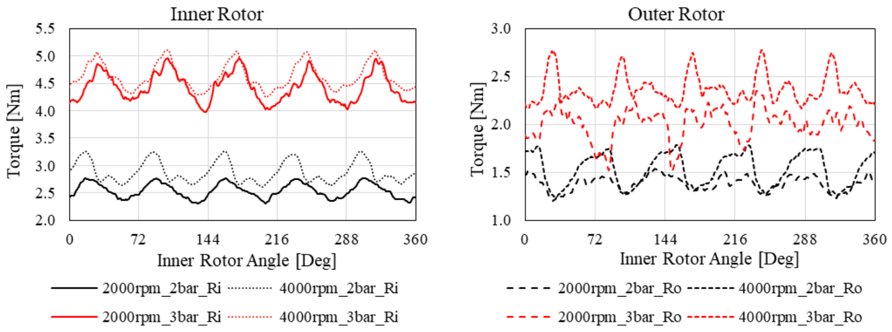

Fig. 7. Rotor torque variation.

4.3 Compressor Performance Analysis

The compressor calculations were performed such that stable pressure and flow distribution is observed. Data from the final five flow cycles was averaged to evaluate the performance of the compressor, presented in Table 3 for the various operating conditions. The air flow and indicated power variation with inner rotor speed is presented in Fig. 8. Specific power, efficiency and discharge temperature data is presented in Fig. 9.

Table 3. 5-6 IGSC performance results.

Discharge Pressure	Inner Rotor Speed	Air Flow Rate	Power	Volumetric Efficiency	Oil Flow Rate	Air-to-Oil Mass Ratio	Discharge Temperature	Specific Power	Isentropic Efficiency
[kPa]	[rpm]	[m³/min]	[W]	[%]	[kg/min]	[-]	[C]	[kW/m³/min]	[%]
200	1000	0.140	360.97	62.05	1.321	0.12	53.3	2.585	49.4
200	2000	0.349	774.03	77.46	1.562	0.26	72.5	2.221	57.5
200	3000	0.601	1227.71	89.09	2.188	0.32	81.5	2.042	62.6
200	4000	0.862	1739.74	95.80	2.864	0.35	101.5	2.018	63.3
300	2000	0.320	1278.49	71.11	3.543	0.11	71.6	3.995	53.8
300	3000	0.548	1995.40	81.17	4.176	0.15	83.4	3.642	59.1
300	4000	0.808	2763.79	89.82	5.560	0.17	94.4	3.419	62.9

Air Flow. As shown in Fig. 8a, at 1000 rpm, 200 kPa discharge pressure, the flow through the compressor is 0.14 m^3/min. As the speed increases, there is a proportional increase in the flow to 0.862 m^3/min at 4000 rpm. With increase in pressure to 300 kPa, there is a reduction in the air flow which is 0.32 m^3/min at 2000 rpm and increases to 0.808 m^3/min at 4000 rpm.

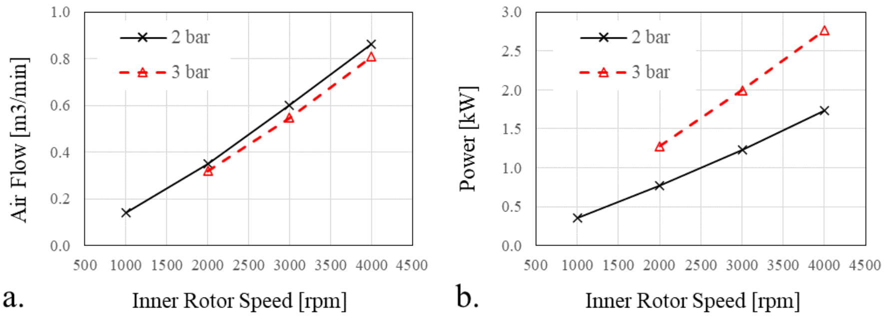

Fig. 8. Air flow and Indicated power.

Indicated Power. Similarly, from Fig. 8b, at 1000 rpm, 200 kPa discharge pressure, compressor's indicated power is the lowest at 360 W. As the speed increases, the indicated power increases to 1.74 kW at 4000 rpm. This is also seen in the internal pressure distribution from Fig. 6. At higher discharge pressure of 300 kPa there is significant increase in power. With 1.28 kW at 2000 rpm, it increases to 2.76 kW at 4000 rpm.

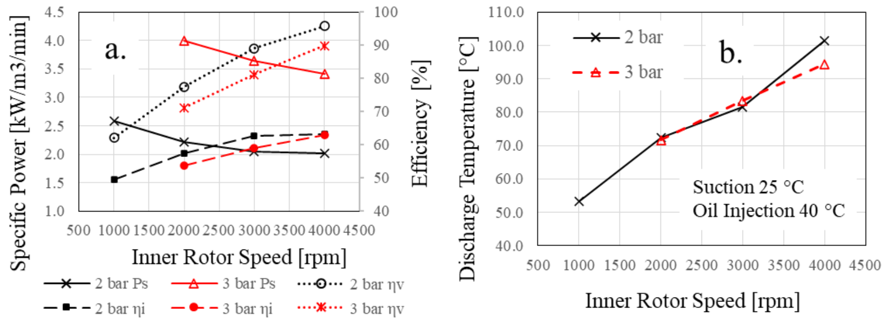

Fig. 9. Specific indicated power, volumetric and isentropic efficiency, and discharge temperature.

Specific Power. Plot of specific power in Fig. 9a shows that the lowest specific power is 2.0 kW/m^3/min at 4000 rpm, 200 kPa pressure. Both flow and indicated power have increased at 4000 rpm, however the increase in flow is more as compared to the increase in power. This results in a better specific power. At 1000 rpm, 200 kPa the specific power increases to 2.6 kW/m^3/min. At 300 kPa, overall specific power is higher and varies from 4.0 kW/m^3/min at 2000 rpm to 3.42 kW/m^3/min at 4000 rpm.

Volumetric and Isentropic Efficiencies. Plots of volumetric and isentropic efficiencies of the compressor are also presented in Fig. 9a. The volumetric efficiency is maximum of 95% at 4000 rpm, 200 kPa pressure. At 2000 rpm is drops down 33%. At 300 kPa pressure, the volumetric efficiency varies from 71% at 2000 rpm to close to 90%

at 4000 rpm. For a small size of the IGSM, this volumetric efficiency is in an acceptable range and can be improved further by clearance control and improvement to the oil injection. Due to oil injection heat transfer and leakage flow re-compression effects, the isentropic efficiency of the compressor is in a lower range from 50 to 63 %.

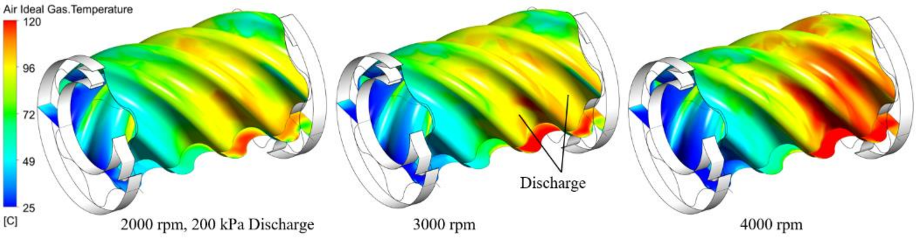

Fig. 10. Instantaneous air temperature at various operating speeds.

Air Temperature. The suction air temperature was set to 25 °C. During the compression temperature rises. The leakage of gas also contributes to further rise in chamber temperature due to re-compression. Oil injection temperature was set to 40 °C, 30° after the closure of suction, so initial heat transfer rate depends on the difference between local gas temperature, and this injected oil. Local air temperature in the compression chamber can be highly non-uniform as seen in Fig. 10. Fig. 10 is a comparison of the instantaneous temperature distribution on the inner rotor at 200 kPa pressure and speed of 2000, 3000 and 4000 rpm. It can be seen from Fig. 10 that the temperature ranges from 25 to 120 °C. The cycle average discharge temperature was lower than this local peak as seen in Fig. 9b. As the speed increases, there is an increase in the quantity of oil getting injected (Table 3), however the mass of oil distributed into each chamber has reduced, together with the time available for heat transfer between oil and air. This results into an increase in the air temperature with speed.

4.4 Port Flow Dynamics

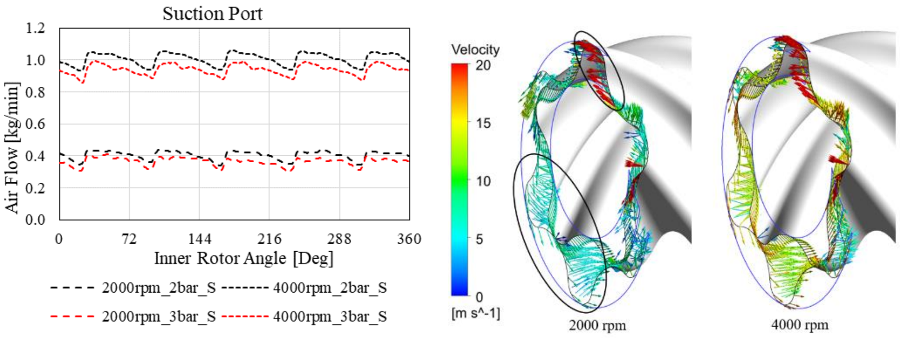

Fig. 11. Air flow pulsation at the suction port and gas velocity distribution.

Suction Flow. The suction port spans from the root of the inner rotor to the tip of the outer rotor and can connect 2 to 3 chambers over its circumference. As the rate of change of volume can vary between successive chambers, the distribution of air within the port is highly non-uniform and turbulent. The cyclic variation of suction flow over a rotation of the inner rotor is presented in Fig. 11. Fig. 11 also shows an instantaneous velocity distribution in the port at 200 kPa, 2000 and 4000 rpm. At both speeds, the flow with 300 kPa pressure is lower than at 200 kPa. The average flow increases from 0.4 kg/min at 2000 rpm to 0.9 kg/min at 4000 rpm. The flow velocity is seen to increase from 6 m/s at 2000 rpm to 12 m/s at 4000 rpm. At locations of axial leakage, the velocity of gas exceeds 20 m/s.

Discharge flow. Circumference of the discharge port is smaller and covers only 1 – 2 chambers simultaneously. The presence of a differential pressure between the chamber and the ports creates a very non-uniform flow field in the discharge ports. High magnitude pulsations are experienced. The cyclic variation of suction flow over a rotation of the inner rotor is presented in Fig. 12, together with an instantaneous velocity distribution in the port at 200 kPa, 2000 and 4000 rpm. In Fig. 6, over-compression and under-compression was observed with 200 kPa and 300 kPa pressure respectively. This causes a strong flow reversal in the discharge port in case of 300 kPa as shown in Fig. 12. At both pressures, pulsation of the flow is stronger at 4000 rpm. From the velocity distribution, the flow velocity is seen to increase from 10 m/s at 2000 rpm to 18 m/s at 4000 rpm. At locations of axial leakage, the velocity of gas exceeds 20 m/s.

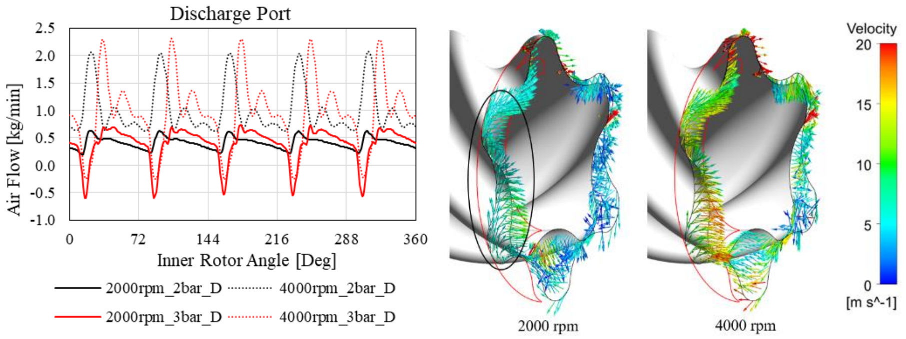

Fig. 12. Air flow pulsation at the discharge port and gas velocity distribution.

Oil Injection Flow. The oil injection port is located on the high-pressure end plate. Due to the movement of the rotors, the injection hole is blocked from the chamber during operation and the flow is intermittent in nature. The formation of the oil pattern within the chamber is presented in Fig. 13 over a complete cycle of 72°. With a reference of zero as closure of the suction port, the oil injection is timed to start at 30°. As the rotors move and the chamber is exposed, oil starts flowing in axial direction, comes in contact with the outer rotor surface and is pushed radially inwards towards the inner rotor surface (seen at 45°). At 60°, injection hole is disconnected from the chamber. On further rotation, oil contacting inner rotor surface is seen at 75° and the patch area keeps increasing. At 102°, the next oil injection cycle begins into the successive chamber.

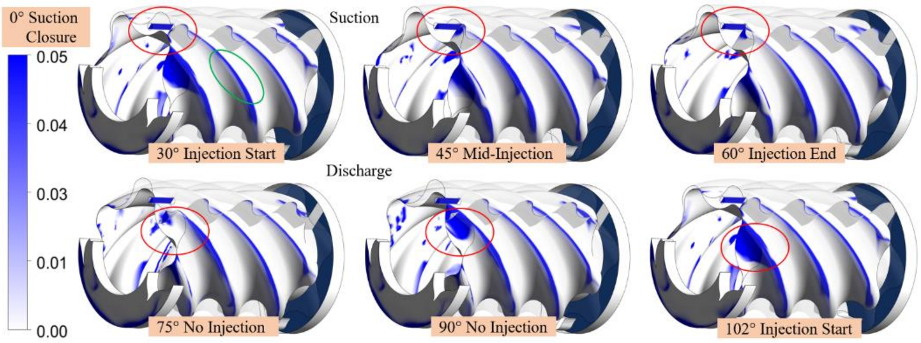

Fig. 13. Oil injection pattern over a cycle.

5 Conclusions

A prototype design of a 5-6 IGSM compressor for air, with oil injection has been analysed using a custom developed numerical grid. A two-fluid Eulerian-Eulerian CFD model has been applied for the calculations. Compressor performance at various operating conditions has been evaluated together with an analysis of the flow at the suction, discharge, and injection ports. Over the calculated range of speed and pressure, a specific power of 2 – 4 kW/m^3/min was estimated with a maximum volumetric efficiency of 95%. The adopted CFD model could be further used to optimize the oil injection and evaluate design modifications such as rotor profiles and lead of the rotors.

Acknowledgments Funding for this research was received from Carrier Corporation, USA and PDM Analysis Ltd., UK.

References

1. Read, M.: Basic design procedure for an internally geared screw compressor. IOP Conf. Ser.: Mater. Sci. Eng. **1180** 012055 (2021). doi: 10.1088/1757-899X/1180/1/012055
2. Read, M., Smith, I. K., Stosic, N.: Influence of rotor geometry on tip leakage and port flow areas in gerotor-type twin screw compressors. Proc of the IMechE, Part E: Journal of Process Mechanical Engineering. 236(1), 94-102 (2022). doi:10.1177/0954408920962412
3. Rane, S., Kovacevic, A.: Algebraic generation of single domain computational grid for twin screw machines. Part I. Implementation, Advances in Engineering Software, 107, 38-50 (2017). doi: 10.1016/j.advengsoft.2017.02.003.
4. Rane, S.: Grid Generation and CFD Analysis of Variable Geometry Screw Machines. Doctoral Thesis. City, University of London (2015).
5. Rane, S., Kovacevic, A., Stosic, N.: CFD Analysis of Oil Flooded Twin Screw Compressors. Int Compressor Engineering Conference, Purdue, 11023 (2016).